Journal of Power Sources 189 (2009) 1247–1250

Contents lists available at ScienceDirect

Journal of Power Sources

journal homepage: www.elsevier.com/locate/jpowsour

Short communication

Microstructural investigation and electrochemical property of $Mg_{63}Ni_{27}Nd_{10}$ amorphous alloy

Lin-jun Huang[a,*], Jian-guo Tang[a], G.Y. Liang[b], Yao Wang[a], D.C. Wu[b]

[a] College of Chemistry, Chemical and Environmental Engineering, Qingdao University, Qingdao 266071, China
[b] Department of Materials Physics, Science school, State Key Laboratory of Mechanical Behavior for Materials, Xi'an Jiaotong University, Xi'an 710049, China

ARTICLE INFO

Article history:
Received 5 August 2008
Received in revised form
29 November 2008
Accepted 1 December 2008
Available online 6 December 2008

Keywords:
Amorphous alloy
Microstructure
Hydrogenation
Discharge capacity

ABSTRACT

Amorphous Mg-based alloy $Mg_{63}Ni_{27}Nd_{10}$ was prepared by melt-spinning. The phase structures and the electrochemical properties of the ribbons before and after charge/discharge cycling were characterized by high-resolution transmission electron microscopy (HRTEM), X-ray diffraction (XRD) analysis and galvanotactic charge–discharge cycle test, respectively. It was found that the amorphous structure begins to crystallize after four cycles of hydrogenation/dehydrogenation and a new nano-crystallized phase $NdMg_2Ni_9$ was detected with average grain size in the range 5–10 nm. A good cycle life and high discharge capacity were also observed in the $Mg_{63}Ni_{27}Nd_{10}$ alloy electrode. The highest discharge capacity reached 580.5 mAh g^{-1} at the discharge current densities of 50 mA g^{-1}. It is suggested that homogeneous microstructure contributes to the enhancement in electrochemical characteristics, the presence of $NdMg_2Ni_9$ being beneficial for the improvement in cycle life of $Mg_{63}Ni_{27}Nd_{10}$ alloy electrode.
© 2008 Elsevier B.V. All rights reserved.

1. Introduction

Mg-based hydrogen storage alloys are considered as one of the most promising candidates of third generation alloys, because of their high discharge capacity, lower density and rich natural resources [1–3]. However, the practical application of Mg-based alloys is prevented by their poor hydriding/dehydriding kinetics at room temperature and their poor charge/discharge cycling stability. In order to extend the cycle life and increase the discharge capacity, many efforts have been made to improve their electrochemical characteristics. In recent years, special attention has been given to the microstructure of the electrode and the amorphous structure was known as a key factor to achieve high discharge capacity and good cycling stability for its special disordered atomic packing and good corrosion resistance [4–6].

However, the amorphous structure is unstable and would be crystallized with the proceeding of charge/discharge cycles. In addition, details of the microstructure evolution of Mg-based amorphous alloys processed by hydrogenation/dehydrogenation are not clear. Therefore, how to retain the amorphous structure of the electrode or postpone the crystallization of the amorphous electrode materials becomes very important in future studies.

In a series of our previous papers the crystallization, microstructure and the hydrogen storage properties for various rapidly Mg-based amorphous alloys were studied [7–9]. This paper is a further study aiming to give a detailed investigation on the electrochemical property and microstructure evolution of amorphous $Mg_{63}Ni_{27}Nd_{10}$ alloy processed by hydrogenation/dehydrogenation, and the effects of microstructure on the discharge capacity are also discussed.

2. Experimental

$Mg_{63}Ni_{27}Nd_{10}$ alloy ingot was prepared by induction melting a mixture of pure Nd metal and Mg–Ni alloy in a vacuum furnace under the protection of argon gas. Based on the low melting point and the high vapor pressure of Mg, a special melting technique, using positive pressure protection and repeated melting, has been used to prevent massive Mg evaporation and ensure composition homogeneity during master alloy ingot preparation. The amorphous ribbons were produced by a single roller melt-spun technique (copper quenching disc with a diameter of 250 mm and surface velocity of about 39 m s^{-1}) in a argon atmosphere of 400 mbar. The ribbons were about 2 mm wide and 20 μm thick.

In electrochemical measurement, the amorphous alloy ribbons were fixed in a special mold to form the negative electrode. The positive electrode was made of Ni-oxyhydroxide/dihydroxide. The alkaline solution was 6 mol l^{-1} KOH containing 20 g l^{-1} LiOH. The specimens were charged at 100 mA g^{-1} for 12 h and discharged

* Corresponding author. Tel.: +86 532 85951961; fax: +86 532 85951519.
E-mail address: newboy66@126.com (L.-j. Huang).

0378-7753/$ – see front matter © 2008 Elsevier B.V. All rights reserved.
doi:10.1016/j.jpowsour.2008.12.001

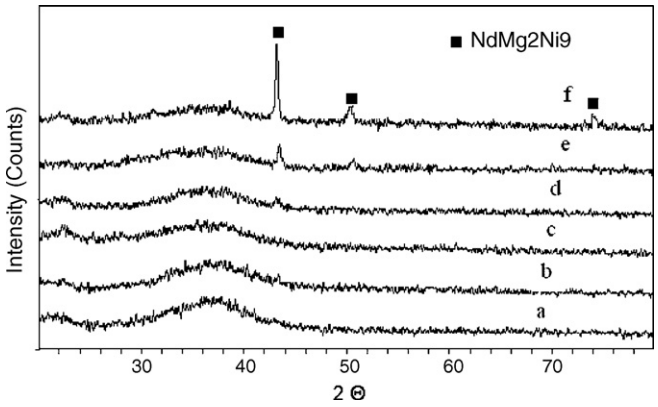

Fig. 1. XRD patterns of amorphous $Mg_{63}Ni_{27}Nd_{10}$ samples charge/discharge for: (a) one cycle; (b) two cycles; (c) three cycles; (d) four cycles; (e) five cycles; (f) six cycles.

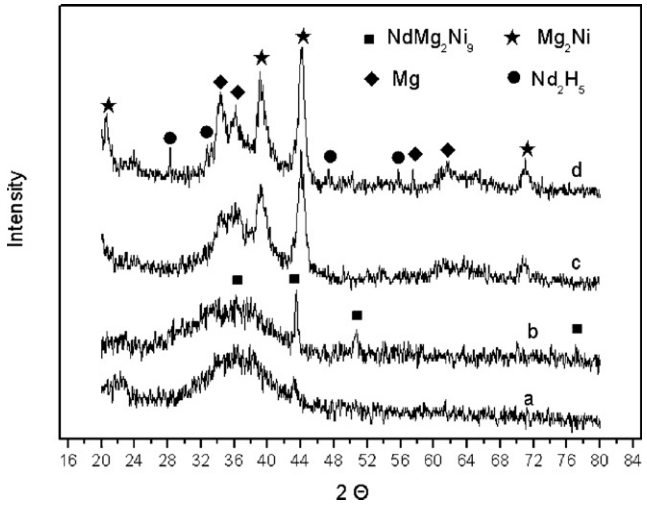

Fig. 2. XRD patterns of amorphous samples $Mg_{63}Ni_{27}Nd_{10}$ charge/discharge for: (a) 5 cycles; (b) 6 cycles; (c) 10 cycles; (d) 20 cycles.

at 50 mA g^{-1} using an Arbin (Texas, America) BTW-2000 battery testing instrument. The discharged cut-off potential was set to 0.8 V between the two electrodes. The resting time between the charge and discharge was 1 h.

The microstructural characterization of the ribbons after charge/discharge cycles was confirmed by high-resolution transmission electron microscopy (HRTEM, JEOL-2010, Japan) and by X-ray (using Cu kα radiation) and electron diffraction.

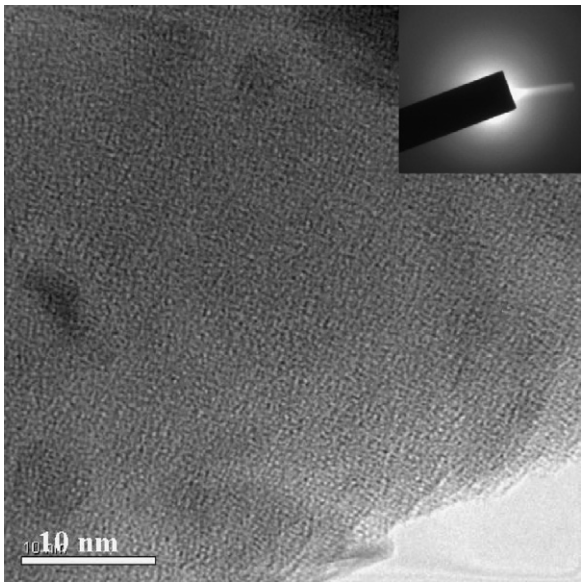

Fig. 3. HRTEM image and electron diffraction pattern of amorphous sample $Mg_{63}Ni_{27}Nd_{10}$ charged/discharged for three cycles.

3. Results and discussion

3.1. Microstructure evolution

The XRD patterns of the amorphous samples that charging/discharging for one to six cycles are presented in Fig. 1. It is seen that after charge–discharge for one to three cycles (Fig. 1a–c) the samples show only a broad and diffuse peak, namely the featureless appearance typical of an amorphous structure. However, after four cycles of hydrogenation/dehydrogenation, the amorphous structure begins to nano-crystallize (see Fig. 1d). By indexing, the nano-crystalline phase $NdMg_2Ni_9$ is detected. The peak of the new phase showed in Fig. 1e and f becomes stronger with increasing charge/discharge cycling, indicating that the new phase $NdMg_2Ni_9$ is growing.

The XRD patterns of the amorphous samples after charging/discharging for 5, 6, 10 and 20 cycles are presented in Fig. 2. It is seen that the amorphous structure gradually crystallized as cycling proceeded. Mg_2Ni phases appeared after 6–10 cycles. After 20 cycles of charging/discharging the stable Mg_2Ni, α-Mg and Nd_2H_5 phases are present (Fig. 2d), indicating that the phase $NdMg_2Ni_9$ formed at beginning is decomposed into phases Mg_2Ni,

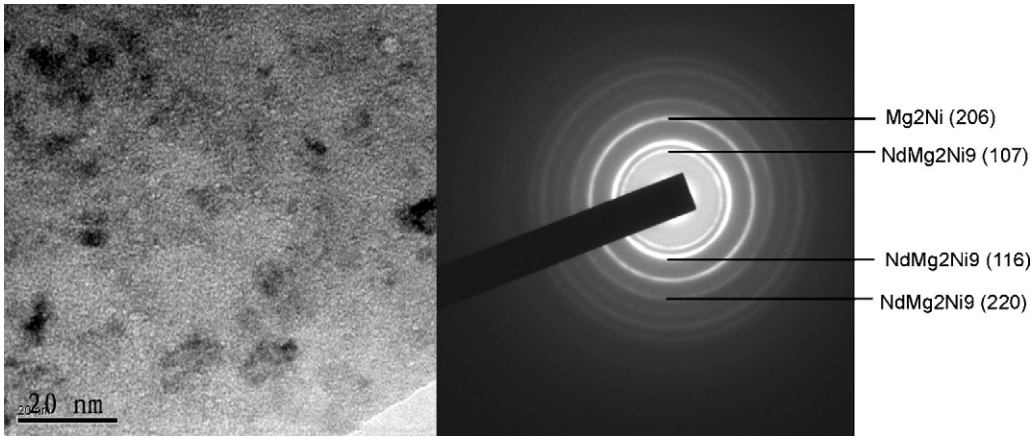

Fig. 4. HRTEM image and electron diffraction pattern of amorphous sample $Mg_{63}Ni_{27}Nd_{10}$ charged/discharged for six cycles.

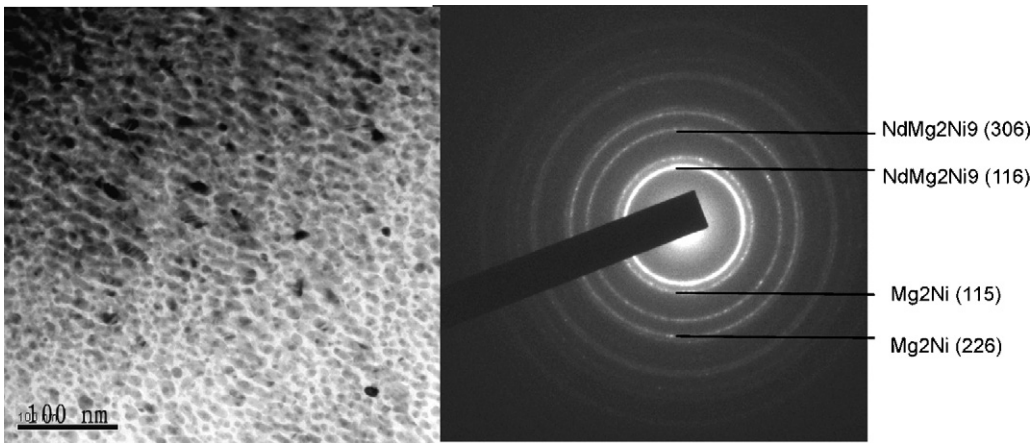

Fig. 5. HRTEM image and electron diffraction pattern of amorphous sample $Mg_{63}Ni_{27}Nd_{10}$ charged/discharged for 10 cycles.

αMg and Nd_2H_5 gradually with the proceeding of hydrogenation/dehydrogenation.

The HRTEM image and electron diffraction pattern of amorphous sample $Mg_{63}Ni_{27}Nd_{10}$ charged/discharged for three cycles are showed in Fig. 3. It is found that a uniform amorphous structure was obtained after three cycles of hydrogenation/dehydrogenation. (The size of short-range order structure in the amorphous is about 0.5 nm).

Fig. 4 shows the HRTEM image and electron diffraction pattern of amorphous sample $Mg_{63}Ni_{27}Nd_{10}$ charged/discharged for six cycles. It is seen that charging/discharging after six cycles for the amorphous samples leads to formation of nano-crystalline phase $NdMg_2Ni_9$ with average grain size in the range 5–10 nm (Figs. 2b and 4) and the nano-size phase Mg_2Ni appears. (The size of short-range order structure in the amorphous phase has then become 1 nm).

Fig. 5 shows the high-resolution transmission electron microscopy images of amorphous sample $Mg_{63}Ni_{27}Nd_{10}$ charged/discharged for 10 cycles. It showed that an amorphous sample charged/discharged in hydrogen over 10 cycles results in nano-crystalline structures with a few residual amorphous phases. Charging/discharging after 10 cycles causes formation of a coarser grained crystalline phase Mg_2Ni with average grain size in the range 10–20 nm (Figs. 2c and 5).

The HRTEM image and electron diffraction pattern of amorphous sample $Mg_{63}Ni_{27}Nd_{10}$ charged/discharged for 20 cycles are shown in Fig. 6. It is found that after 20 cycles of charging/discharging the amorphous samples are almost completely crystallized and stable Mg_2Ni, αMg and Nd_2H_5 phases with the biggest grain size about 100 nm (Fig. 6) are present, indicating that the $NdMg_2Ni_9$ phase formed at beginning is decomposed into Mg_2Ni, αMg and Nd_2H_5 phases gradually with the proceeding of hydrogenation/dehydrogenation (Figs. 2 and 6).

3.2. Electrochemical properties

Fig. 7a shows the variation of the discharge capacity of the $Mg_{63}Ni_{27}Nd_{10}$ sample versus the number of cycles. It can be observed that with increasing cycle number the capacity reached a maximum after three cycles, and then decreased in higher cycles. The largest discharge capacity of the sample reached 580.5 mAh g^{-1} after three cycles, and then decreased for higher cycles. After 10 cycles, capacity falloff was regular. The capacity after 20 cycles (460.9 mAh g^{-1}) reaches 80% of the maximum capacity.

The relationship of discharge potentials (voltage) and the discharge capacities (at the 10th cycle) is shown in Fig. 8. It is seen that there is a discharge potential plateau from 1.3 V to 1.0 V with a

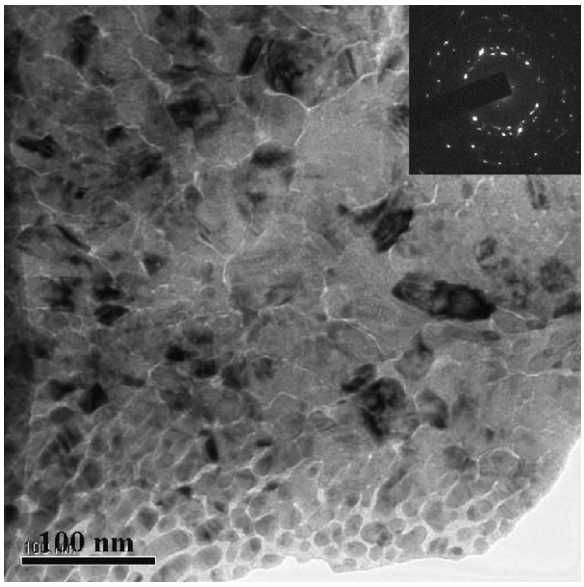

Fig. 6. HRTEM image and electron diffraction pattern of amorphous sample $Mg_{63}Ni_{27}Nd_{10}$ charged/discharged for 20 cycles.

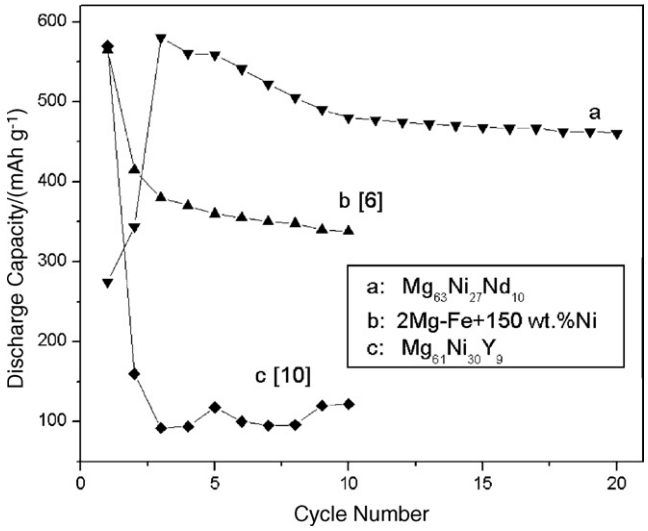

Fig. 7. Variation of the discharge capacity versus cycle number for the different samples.

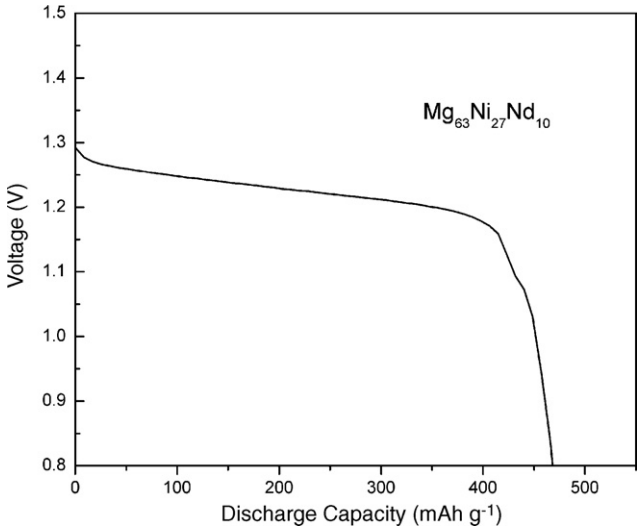

Fig. 8. Relationship of voltage and the discharge capacities (at the 10th cycle).

change in discharge capacity denoting the range over which the alloy may be used. The plateau discharge capacity is more than 480 mAh g^{-1} at the10th cycle.

3.3. Effects of microstructure on discharge capacity

Fig. 7b and c shows the different Mg-based amorphous samples with a high discharge capacity obtained in these investigations. They are 2Mg–Fe + 150 wt.%Ni [6] and $Mg_{61}Ni_{30}Y_9$ [10]. It can be observed that the maximum discharge capacities reached for $Mg_{63}Ni_{27}Nd_{10}$, 2Mg–Fe + 150 wt.%Ni and $Mg_{61}Ni_{30}Y_9$ are, respectively, 580.5, 565.2 and 570mAh g^{-1}, and that $Mg_{63}Ni_{27}Nd_{10}$ has the best cyclic performance among the three samples. For this alloy, discharge capacity reaches a maximum values after two cycles, then decreases. This phenomenon has been observed in other Mg-based hydrogen storage alloys [11,12].

Xuezhang et al. [6] and Khorkounov et al. [10] reported amorphous 2Mg–Fe + 150 wt.%Ni and $Mg_{61}Ni_{30}Y_9$ ribbons synthesized by mechanical alloying. From the above results, it is evident that the melt-spun ribbon $Mg_{63}Ni_{27}Nd_{10}$ showed superior hydrogenation kinetics and higher discharge capacity. One explanation for this could be the homogeneous microstructure of the melt-spun alloy. The as-cast eutectic alloy charged/discharged for some cycles consisted of lamellae of primary and secondary phases (see Figs. 2 and 5), where long continuous boundaries between primary and secondary phases could act as diffusion paths prior to hydrogen diffusion into the bulk. Zhu et al. [13] also reported that an auto-catalytic effect is might govern the hydriding mechanism of the nanophase composite, while the hydriding process of single component alloys proceeds by means of a nucleation and growth mechanism. Another explanation could be the existence of nano-crystalline phase $NdMg_2Ni_9$ (see Figs. 2, 4 and 5). The new ternary Mg-based hydrogen storage alloys, RMg_2Ni_9 (where R = La, Ce, Pr, Nd, Sm and Gd), were first reported by Kadir et al. [14] in 1997, and the latest investigations of the RMg_2Ni_9 hydrogen storage alloys suggested that the new ternary alloys may be regarded as the most promising candidate for possible improvement because of their special structure for hydrogen storage [15–18]. From the above results, after four cycles of hydrogenation/dehydrogenation, the amorphous structure begins to nano-crystallize (see Figs. 1(d) and 4) and a nano-crystallized phase $NdMg_2Ni_9$ is present, rapidly leading to a very high discharge capacity (see Fig. 7a). In addition, the amorphous phase embedding the nanocrystalling grains in the melt-spun material (see Figs. 4 and 5) may provide fast bulk diffusion of hydrogen because of the lower atomic density in the amorphous state. According to the results of Orimo et al. [19] reported, hydrogen concentrations in the grain boundaries are much higher than that in the grain interior and amorphous regions. The formation of nanocrystalline grains increases the grain boundary in the melt-spun ribbon sample, which no doubt promotes its hydrogen storage properties.

4. Conclusions

A detailed investigation on the microstructural evolution of amorphous $Mg_{63}Ni_{27}Nd_{10}$ alloy processed by hydrogenation/dehydrogenation has been given, and the effects of microstructure on the discharge capacity are also discussed. The results obtained are summarized as follows:

1. After four cycles of hydrogenation/dehydrogenation, the amorphous structure of $Mg_{63}Ni_{27}Nd_{10}$ alloy begins to crystallize and a nano-crystalline phase $NdMg_2Ni_9$ is detected with average grain size in the range 5–10 nm. Nano-size Mg_2Ni phases appear after 6–10 cycles.
2. After 20 cycles of charging/discharging stable Mg_2Ni, αMg and Nd_2 H_5 phases are present, indicating that the $NdMg_2Ni_9$ phase formed at beginning gradually decomposes into Mg_2Ni, αMg and Nd_2H_5 phases as hydrogenation/dehydrogenation proceeds.
3. In the electrochemical property measurements, the highest discharge capacity reached 580.5 mAh g^{-1} at a discharge current densities of 50 mA g^{-1} for the $Mg_{63}Ni_{27}Nd_{10}$ sample, whose discharge capacity reached 80% of its maximum after 20 cycles. The discharge capacity of the potential plateau (from 1.3 V to 1.0 V) attained more than 480 mAh g^{-1} at 10 cycles.
4. The discharge capacity became lower as crystallization proceeded with loss of the initial amorphous structure. Incorporation of nanocrystalline grains of the melt-spun alloy was a key factor in achieving high discharge capacity and good cycling stability.

Acknowledgements

This study was supported by the Doctoral Foundation of Xi'an Jiaotong University (Grant No. DFXJTU-200516) and National Natural Science Foundation of China (Grant No. 50371066).

References

[1] J.C. Bolcich, A.A. Yawuy, H.L. Corso, H.A. Pertti, C.O. Anala, Int. J. Hydrogen Energy 19 (1994) 605.
[2] N. Cui, B. Luan, H.J. Zhao, H.K. Liu, S.X. Dou, J. Power Source 55 (1995) 263.
[3] L. Schlapbach, A. ZÜttel, Nature 414 (2001) 353.
[4] J.-W. Liu, L.-F. Jiao, H.-T. Yuan, Y.-J. Wang, Q. Liu, J. Alloys Comp. 403 (2005) 270.
[5] B. Khorkounov, A. Gebert, Ch. Mickel, L. Schultz, J. Alloys Comp. 416 (2006) 110.
[6] X. Xiao, X. Wang, L. Gao, L. Wang, C. Chen, J. Alloys Comp. 413 (2006) 312.
[7] L.J. Huang, G.Y. Liang, Z.B. Sun, J. Alloys Comp. 421 (2006) 279.
[8] L.J. Huang, G.Y. Liang, Z.B. Sun, Y.F. Zhou, D.C. Wu, Mater. Sci. Eng. B 141 (2007) 121–125.
[9] L.J. Huang, G.Y. Liang, Z.B. Sun, Y.F. Zhou, J. Alloys Comp. 432 (2007) 172.
[10] B. Khorkounov, A. Gebert, Ch. Mickel, L. Schultz, J. Alloys Comp. 458 (2008) 479.
[11] S. Orimo, H. Fujii, K. Ikeda, Acta Mater. 45 (1997) 331.
[12] W.H. Liu, H.Q. Wu, Y.Q. Lei, J. Alloys Comp. 252 (1997) 234.
[13] M. Zhu, Y. Gao, Z.X. Che, Y.Q. Yang, C.Y. Chuang, J. Alloys Comp. 330–332 (2002) 708.
[14] K. Kadir, T. Sakai, I. Uehara, J. Alloys Comp. 257 (1997) 115.
[15] K. Kadir, T. Sakai, I. Uehara, J. Alloys Comp. 302 (2000) 112.
[16] Z.M. Wang, H.Y. Zhou, G. Cheng, Z.F. Gu, J. Alloys Comp. 384 (2004) 279.
[17] X. Xu, H.Y. Zhou, R.P. Zou, S.L. Zhang, Z.M. Wang, J. Alloys Comp. 396 (2005) 247.
[18] H.Y. Zhou, S.L. Zhang, Q.R. Yao, W.J. Li, J. Alloys Comp. 429 (2007) 116.
[19] S. Orimo, H. Fujii, Appl. Phys. A 72 (2001) 167.